Biophysical Journal Volume 69 December 1995 2298–2303

Calculation of Translational Friction and Intrinsic Viscosity. II. Application to Globular Proteins

Huan-Xiang Zhou
Department of Biochemistry, Hong Kong University of Science and Technology, Clear Water Bay, Kowloon, Hong Kong

ABSTRACT The translational friction coefficients and intrinsic viscosities of four globular proteins (ribonuclease A, lysozyme, myoglobin, and chymotrypsinogen A) are calculated using atomic-level structural details. Inclusion of a 0.9-Å-thick hydration shell allows calculated results for both hydrodynamic properties of each protein to reproduce experimental data. The use of detailed protein structures is made possible by relating translational friction and intrinsic viscosity to capacitance and polarizability, which can be calculated easily. The 0.9-Å hydration shell corresponds to a hydration level of 0.3–0.4 g water/g protein. Hydration levels within this narrow range are also found by a number of other techniques such as nuclear magnetic resonance spectroscopy, infrared spectroscopy, calorimetry, and computer simulation. The use of detailed protein structures in predicting hydrodynamic properties thus allows hydrodynamic measurement to join the other techniques in leading to a unified picture of protein hydration. In contrast, earlier interpretations of hydrodynamic data based on modeling proteins as ellipsoids gave hydration levels that varied widely from protein to protein and thus challenged the existence of a unified picture of protein hydration.

INTRODUCTION

Hydration is essential for the proper functioning of proteins and has thus been under extensive investigations (Kuntz and Kauzmann, 1974; Rupley et al., 1983; Rupley and Careri, 1991). A number of techniques such as nuclear magnetic resonance spectroscopy (Kuntz, 1971), infrared spectroscopy and calorimetry (Rupley et al., 1983), and computer simulation (Steinbach and Brooks, 1993) lead to a unified picture of hydration. A protein is hydrated at a definite level; adding water to a dry protein sample beyond this level produces no further change in protein properties and simply serves to dilute the sample (Rupley and Careri, 1991). For globular proteins, hydration levels are found to fall within a narrow range, between 0.3 and 0.4 g water/g protein (this unit will be omitted from now on).

However, this unified picture seems to be challenged by hydrodynamic measurements. Hydration levels deduced from data on diffusion coefficient and intrinsic viscosity have a much wider range (from 0.14 to 1.04) and in general are much higher (around 0.54) (Kuntz and Kauzmann, 1974; Squire and Himmel, 1979). It should be noted that these hydration levels were based on modeling proteins as ellipsoids, for which the diffusion coefficient and intrinsic viscosity are analytically known. The purpose of this paper is to show that hydration levels deduced from hydrodynamic data actually conform to the unified picture of hydration if the detailed structures of proteins are used.

The use of detailed protein structures is made possible by relations developed in the preceding paper (Zhou, 1995) between hydrodynamic properties and electrostatic properties. It was demonstrated that, for a globular particle, the relation between the translational friction coefficient ξ and the capacitance C,

$$\xi = 6\pi\eta_0 C, \tag{1}$$

is accurate to within about 1% and the relation between the intrinsic viscosity $[\eta]$ and the polarizability α,

$$[\eta] = \frac{3}{4}\alpha + \frac{1}{4}V_p, \tag{2}$$

is accurate to within about 3%. In Eq. 1, η_0 is the viscosity of the solvent; in Eq. 2, V_p is the volume of the particle. The translational friction coefficient ξ gives the diffusion coefficient D through the Stokes-Einstein equation

$$D = k_B T/\xi, \tag{3}$$

where k_B is Boltzmann's constant and T is the temperature. Thus the diffusion coefficient and the intrinsic viscosity of a protein can be found by calculating its capacitance and polarizability. Both C and α of the protein, with its detailed structure taken into consideration, can be obtained in a single calculation using the boundary-element technique (Zhou, 1993, 1994, 1995).

Four globular proteins have been studied: ribonuclease A, lysozyme, myoglobin, and chymotrypsinogen A. The proteins were chosen because reliable structural and hydrodynamic data are available for them. These are listed in Table 1. The diffusion coefficients in the table are those in water at 20°C. At this temperature, the solvent viscosity is η_0 = 0.01009 g/cm/s (Partington, 1951). The unit of the intrinsic viscosity is cm^3/g in Table 1, but is $Å^3$ per protein molecule in Eq. 2. To convert to the former unit, the latter unit needs to be multiplied by $10^{-24}\ N_A/M$, where N_A is Avogadro's number and M is the molecular weight of the protein.

Received for publication 19 June 1995 and in final form 5 September 1995.

Address reprint requests to Dr. Huan-Xiang Zhou, Department of Biochemistry, Hong Kong University of Science and Technology, Clear Water Bay, Kowloon, Hong Kong. Tel.: 852-2358-8704; Fax: 852-2358-1552; E-mail: bchxzhou@uxmail.ust.hk.

0006-3495/95/12/2298/06 $2.00

TABLE 1 Structural and hydrodynamic data of four proteins

	Ribonuclease A	Lysozyme	Myoglobin	Chymotrypsinogen A
Molecular weight	13,690	14,320	17,190	25,660
PDB entry	7rsa (1)	6lyz (2)	1mbo (3)	2cga (4)
D (10^{-7} cm^2/s)	11.2 ± 0.2 (5)	11.2 ± 0.2 (6)	10.3 (7)	9.01–9.48 (8)
$[\eta]$ (cm^3/g)	3.30 ± 0.04 (9)	2.98–3.00 (10, 6)	3.15 (11)	2.5–3.13 (12,13)

Numbers in parentheses are references: (1) Wlodawer et al., 1988; (2) Diamond, 1974; (3) Philips, 1986; (4) Wang et al., 1985; (5) Creeth, 1958; (6) Sophianopoulos et al., 1962; (7) Ehrenberg, 1957; (8) Wilcox et al., 1957; (9) Buzzell and Tanford, 1956; (10) Luzzati et al., 1961; (11) Wyman and Ingalls, 1943; (12) Tanford, 1968; and (13) Schwert, 1951.

There are different strategies for treating hydration water in calculating hydrodynamic properties of proteins. For example, one can include explicit water molecules as a part of a protein (Venable and Pastor, 1988). Then one has to assign positions for the water molecules in some arbitrary way. In this paper we simply represent hydration water by a hydration shell with a uniform thickness ϵ. This is equivalent to increasing the radius of each protein atom by ϵ. A similar approach was taken recently by Allison and Tran (1995) in a study of the electrophoretic mobility of lysozyme. For the current strategy to be viable, experimental values of both the diffusion coefficient and the intrinsic viscosity for each protein should be reproduced by using a single ϵ. The hydration level is then given by $10^{-24} N_A \rho_h \Delta V/M$, where ρ_h is the density of hydration water in units of g/cm^3 and ΔV is the volume of the hydration shell (with the above particular thickness) in units of Å^3. Hydration water has been found to have a somewhat higher density than bulk water, with a value of $\rho_h = 1.104$ g/cm^3 (Bull and Breese, 1968).

CALCULATION METHOD

Through Eqs. 1–3, the problem of calculating diffusion coefficient and intrinsic viscosity becomes one of calculating capacitance and polarizability. The solution of the latter problem using the boundary-element technique has been described in detail previously (Zhou, 1993, 1994, 1995), so only a brief summary is given here.

Both the capacitance C and the polarizability α of a particle are calculated from appropriate charge densities on the particle surface S_p (σ_c for C and σ_i, $i = 1$–3, for α). The capacitance is given by

$$C = \int_{S_p} ds\sigma_c(\mathbf{r}), \tag{4}$$

where ds is the surface area element. The polarizability is given by

$$\alpha = \frac{4\pi}{3} \int_{S_p} ds[r_1\sigma_1(\mathbf{r}) + r_2\sigma_2(\mathbf{r}) + r_3\sigma_3(\mathbf{r})], \tag{5}$$

where r_i, $i = 1$–3, are the Cartesian components of the position vector $\mathbf{r}$. The charge densities all satisfy the integral equation

$$\int_{S_p} ds' \frac{\sigma(\mathbf{r}')}{|\mathbf{r}' - \mathbf{r}|} = h(\mathbf{r}), \quad \mathbf{r} \in S_p. \tag{6}$$

In particular, $\sigma_c(\mathbf{r}) = \sigma(\mathbf{r})$ if $h(\mathbf{r}) = 1$, and $\sigma_i(\mathbf{r}) = \sigma(\mathbf{r})$ if $h(\mathbf{r}) = r_i$. By discretizing the surface S_p into small elements, Eq. 6 is reduced to a matrix equation, which is solved by matrix inversion. The results are then used in Eqs. 4 and 5 to obtain the capacitance and polarizability. In calculating the polarizability, the average over the particle surface for each of the three charge density components should be subtracted from that component to ensure that the net charge on the particle is zero.

When the particle is a protein, discretizing the surface poses a major difficulty. We have described a simple but robust method for discretizing protein surfaces (Zhou, 1993). Some proteins contain internal cavities, and the surfaces of these cavities should not be included as part of the protein surfaces. This problem was not appropriately dealt with previously. Now we have implemented in our boundary-element solution an algorithm developed by Alard and Wodak (1991) for eliminating internal cavities. Details of this implementation are given in the Appendix.

RESULTS

Unless otherwise indicated, results presented below were calculated using heavy atoms only. The atomic radii used were: C, 2.0 Å; N, 1.7 Å; O, 1.5 Å; S, 1.8 Å; Fe, 1.7 Å. The structure 7rsa of ribonuclease A is from a joint x-ray and neutron determination and contains all the hydrogen atoms (Wlodawer et al., 1988). It thus provides an opportunity to study the effect of neglecting hydrogen atoms. The hydrogen atom radius was 1.0 Å. The numbers of surface elements used in the calculations ranged from 2747–3010 for ribonuclease A to 4171–5205 for chymotrypsinogen A. Results were checked against those obtained by using just a quarter as many surface elements, and agreement between them was satisfactory.

Capacitance and diffusion coefficient

The capacitances of ribonuclease A, lysozyme, myoglobin, and chymotrypsinogen A calculated at $\epsilon = 0.6, 0.8, 0.9, 1.0,$

and 1.2 Å are listed in Table 2. For each increase in ϵ by 0.1 Å, the capacitances are found to increase by 0.12–0.13 Å. According to Eq. 1, the capacitance of a protein can be viewed as its hydrodynamic radius, i.e., the radius of a sphere that has the same diffusion coefficient as the protein.

The diffusion coefficients in water at 20°C calculated from Eqs. 1 and 3 are also listed in Table 1. The hydration shell thicknesses that give results consistent with experimental data are ϵ = 0.6, 0.8, and 0.9 Å for ribonuclease A, ϵ = 0.8, 0.9, and 1.0 Å for lysozyme, and ϵ = 0.9 and 1.0 Å for myoglobin. For chymotrypsinogen A, results at the five values of ϵ all fall in the range of experimental data (Wilcox et al., 1957).

Volume, polarizability, and intrinsic viscosity

The volumes and polarizabilities and the resulting intrinsic viscosities of the four proteins at the five values of ϵ are listed in Table 3. At each ϵ, the order of the intrinsic viscosities is ribonuclease A > myoglobin > lysozyme ≈ chymotrypsinogen A, in agreement with experiment (see Table 1). The hydration shell thicknesses that give results consistent with experimental data on intrinsic viscosity are ϵ = 0.9 and 1.0 Å for ribonuclease A, ϵ = 0.8 and 0.9 Å for lysozyme, and ϵ = 0.9 and 1.0 Å for myoglobin. For chymotrypsinogen A, all five values of ϵ are acceptable.

Combining results on both diffusion coefficient and intrinsic viscosity, one finds that the hydration shell thickness should be around 0.9 Å for ribonuclease A, around 0.8–0.9 Å for lysozyme, between 0.9 and 1.0 Å for myoglobin, and between 0.6 and 1.2 Å for chymotrypsinogen A.

Effect of neglecting hydrogen atoms

Calculations on ribonuclease A were also made using all atoms of the protein. At ϵ = 0.8 Å, the capacitance was found to be 19.15 Å, compared to 19.11 Å without hydrogen atoms. The volumes with and without hydrogen atoms were 20,388 Å^3 and 20,220 Å^3, and the polarizabilities with and without hydrogen atoms were 90,636 Å^3 and 90,048 Å^3.

TABLE 2 Capacitances and diffusion coefficients of four proteins calculated at five values of hydration-shell thickness

ϵ(Å)	Ribonuclease A	Lysozyme	Myoglobin	Chymotrypsinogen A
			C (Å)	
0.6	18.85	18.65	20.13	22.67
0.8	19.11	18.91	20.39	22.93
0.9	19.24	19.03	20.52	23.06
1.0	19.37	19.16	20.64	23.19
1.2	19.62	19.40	20.89	23.45
			D (10^{-7} cm^2/s)	
0.6	**11.29**	11.41	10.57	**9.384**
0.8	**11.13**	**11.25**	10.43	**9.277**
0.9	**11.06**	**11.18**	**10.37**	**9.225**
1.0	10.98	**11.11**	**10.31**	**9.172**
1.2	10.84	10.96	10.18	**9.074**

Results consistent with experimental data are in boldface.

TABLE 3 Polarizabilities, volumes, and intrinsic viscosities of four proteins calculated at five values of hydration-shell thickness

ϵ(Å)	Ribonuclease A	Lysozyme	Myoglobin	Chymotrypsinogen A
			V_p (Å^3)	
0.6	18,726	19,434	24,889	35,488
0.8	20,220	20,940	26,801	38,057
0.9	20,941	21,668	27,631	39,190
1.0	21,653	22,349	28,444	40,303
1.2	23,056	23,694	30,022	42,476
			α (Å^3)	
0.6	85,502	82,917	104,419	146,022
0.8	90,048	86,159	108,444	150,823
0.9	91,691	87,640	110,288	153,540
1.0	93,833	89,321	112,353	156,646
1.2	97,785	93,000	116,599	162,218
			[η] (cm^3/g)	
0.6	3.03	2.82	2.96	**2.78**
0.8	3.19	**2.94**	3.08	**2.88**
0.9	**3.26**	**2.99**	**3.14**	**2.93**
1.0	**3.33**	3.05	**3.20**	**2.99**
1.2	3.48	3.18	3.33	**3.10**

Results consistent with experimental data are in boldface.

Consequently the errors in the diffusion coefficient and the intrinsic viscosity due to using heavy atoms only were 0.2% and 0.7%, respectively. Thus the effect of neglecting hydrogen atoms is quite small.

Hydration level

As we have just seen, comparison of calculated and experimental results on diffusion coefficient and intrinsic viscosity shows that the hydration shell thicknesses of the four proteins are all around 0.9 Å. Without hydration (ϵ = 0), the volumes of ribonuclease A, lysozyme, myoglobin, and chymotrypsinogen A are V_0 = 12718, 13334, 17275, and 24441 Å^3, respectively. From the volumes of the hydrated proteins listed in Table 3, one finds that, at ϵ = 0.9 Å, the volumes of the four hydration shells are ΔV = 8223, 8334, 10,356, and 14,749 Å^3. The resulting hydration levels are 0.40, 0.39, 0.40, and, 0.38 for the four proteins.

Except for ribonuclease A, comparison with experimental data gives a range of possible values rather than a unique value of hydration shell thickness. The corresponding hydration levels are calculated to be 0.35–0.39 for lysozyme, 0.40–0.43 for myoglobin, and 0.29–0.47 for chymotrypsinogen A.

DISCUSSION

We have shown that inclusion of a hydration shell around 0.9 Å thick allows the calculated diffusion coefficient and intrinsic viscosity for each of four globular proteins to reproduce experimental data. The corresponding hydration levels are in a narrow range (i.e., 0.3–0.4). This is consistent with the finding of a number of other techniques. Hydrodynamic measurement is thus now shown to join the other

techniques in leading to a protein hydration picture that is unified both from probe to probe and from protein to protein.

It should be emphasized that this conclusion is drawn after the use of detailed protein structures in predicting hydrodynamic properties. Earlier interpretations of hydrodynamic data based on modeling proteins as ellipsoids gave hydration levels that varied widely from protein to protein (from 0.14 to 1.04) and in general were much higher (around 0.54) (Kuntz and Kauzmann, 1974; Squire and Himmel, 1979). Part of the error may be due to estimating the molecular volume V_0 of a protein from its partial specific volume $\bar{v}$. The use of $10^{24}\ \bar{v}M/N_A$ has long been criticized (Scheraga, 1961) and indeed we find it to be quite different from V_0. The partial specific volumes of ribonuclease A, lysozyme, myoglobin, and chymotrypsinogen A are 0.703, 0.705, 0.743, and 0.721 cm^3/g, respectively (Richards and Wyckoff, 1971; Sophianopoulos et al., 1962; Ehrenberg, 1957; Schwert, 1951). The molecular volumes estimated from them are $10^{24}\ \bar{v}M/N_A$ = 15,982, 16,765, 21,209, and 30,722 $Å^3$, respectively, and are 23–26% higher than the actual molecular volumes. If actual molecular volumes are used, deduced hydration levels will be lower by similar percentages. However, even then the wide range in deduced hydration levels still points to the inadequacy of ellipsoid models.

In this study, hydration water was simply modeled by a uniform hydration shell. Other strategies are worth exploring. For example, the use of explicit water molecules may provide further information. In addition, it is desirable to extend the present study to other types of macromolecules to gain insight into their hydration.

APPENDIX: ELIMINATION OF CAVITY SURFACES

The basic idea of the Alard and Wodak (1991) algorithm for eliminating internal cavities of a protein is as follows. Geometrically a protein is a collection of interpenetrating spheres (representing individual atoms). The exposed patches (spherical polygons) of the spheres can be generated and sorted into sets of disconnected surfaces. One of them is the outer surface and the rest are the surfaces of all the internal cavities. The fact that the outer surface consists of the largest number of spherical polygons then allows it to be selected and the other surfaces to be eliminated. The above outline is implemented in the following five steps. The exposed spherical polygons are generated through the first three steps and sorted in the fourth step, and the outer surface is selected in the fifth step.

Generation of intersection circles

For easy reference, each of the constituent spheres of the protein is assigned an identity number (e.g., sphere n). The border spheres of sphere n, i.e., those that intersect with it, can be found by comparing intersphere distances and sums of sphere radii. The resulting intersection circles are all assigned to sphere n and numbered consecutively. As illustrated in Fig. 1, each (e.g., the kth) intersection circle of sphere n is assigned a direction, given by the unit vector $\mathbf{e}(n, k)$ pointing from the center of sphere n to the center of the border sphere (say, sphere m) that shares the kth intersection circle with sphere n.

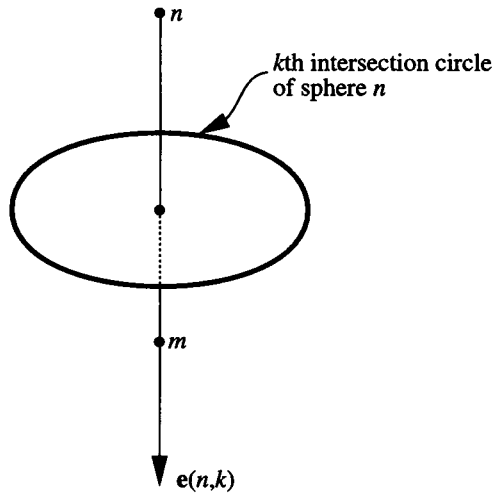

FIGURE 1 An intersection circle of sphere n. The kth intersection circle of sphere n is characterized by the unit vector $\mathbf{e}(n, k)$ pointing from the center of sphere n to the center of sphere m, which shares the kth intersection circle with sphere n. The centers of the two spheres and the center of the intersection circle are marked by black dots.

Generation of exposed arcs on intersection circles

The kth intersection circle is checked against each of the border spheres (except for sphere m) of sphere n to see if a part or all of it is buried. The arcs that are exterior to individual border spheres are numbered consecutively. Suppose the jth arc is exterior to sphere l (see Fig. 2). It is characterized by the vector $\mathbf{u}(n, k, j)$ from the center of the kth intersection circle to the arc's starting point (in the clockwise sense when looking along the direction of $\mathbf{e}(n, k)$) and the spanning angle $\phi(n, k, j)$. For later use, the identity number of the sphere (besides spheres n and m) that is in contact with the starting point of the arc is recorded by $a_1(n, k, j)$. For the present case, $a_1(n, k, j) = l$. Similarly, $a_2(n, k, j)$ is used to record the identity number of the sphere (again sphere l) that is in contact with the ending point of the jth arc on the kth intersection circle of sphere n.

Two special cases exist. The first is that the kth intersection circle of sphere n may be completely buried in the border spheres of sphere n. In this case the intersection circle no longer needs to be considered. The second possibility is that the kth intersection circle is not buried in the border

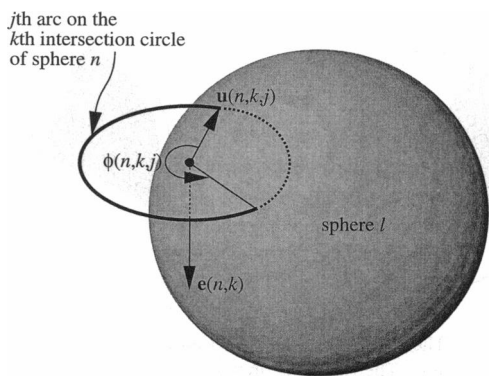

FIGURE 2 The attributes of an exterior arc. The jth arc on the kth intersection circle of sphere n is characterized by the vector $\mathbf{u}(n, k, j)$ from the center of the intersection circle to the arc's starting point and the spanning angle $\phi(n, k, j)$.

spheres at all. In this case the intersection circle is completely exposed. This case needs no further consideration in this step.

If several arcs on the kth intersection circle survive the test against the individual border spheres of sphere n, there is then the possibility that a part or all of the jth exterior arc is buried in another border sphere (say, sphere l'). Let the arc that is exterior to sphere l' be the j'th one on the kth intersection circle. A part or all of the j'th exterior arc may also be buried in sphere l. Both the part of the jth arc that is buried in spheres l' and the part of the j'th arc that is buried in spheres l can be most conveniently eliminated by directly comparing the two arcs. Depending on the relative locations of the two arcs on the intersection circle, six possibilities exist, all of which are shown in Fig. 3. The common parts of the two arcs are not buried in either sphere l' or sphere l. For each surviving arc, the identity numbers of the spheres (besides spheres n and m) that are in contact with the starting and ending points of the arc are recorded by a_1 and a_2, respectively.

These surviving arcs are then tested further against other (i.e., besides m, l, and l') border spheres of sphere n to eliminate buried parts. Such an iterative test eventually allows all the buried parts of the kth intersection circle to be eliminated. The exposed arcs from all the intersections of sphere n are then collected together and numbered consecutively. For each (e.g., the jth) of them, the identity number of the sphere that shares the particular intersection circle with sphere n is recorded by $a_0(n, j)$ and the identity numbers of the spheres (besides spheres n and a_0) that are in contact with the starting and ending points of the arc are recorded by $a_1(n, j)$ and $a_2(n, j)$, respectively.

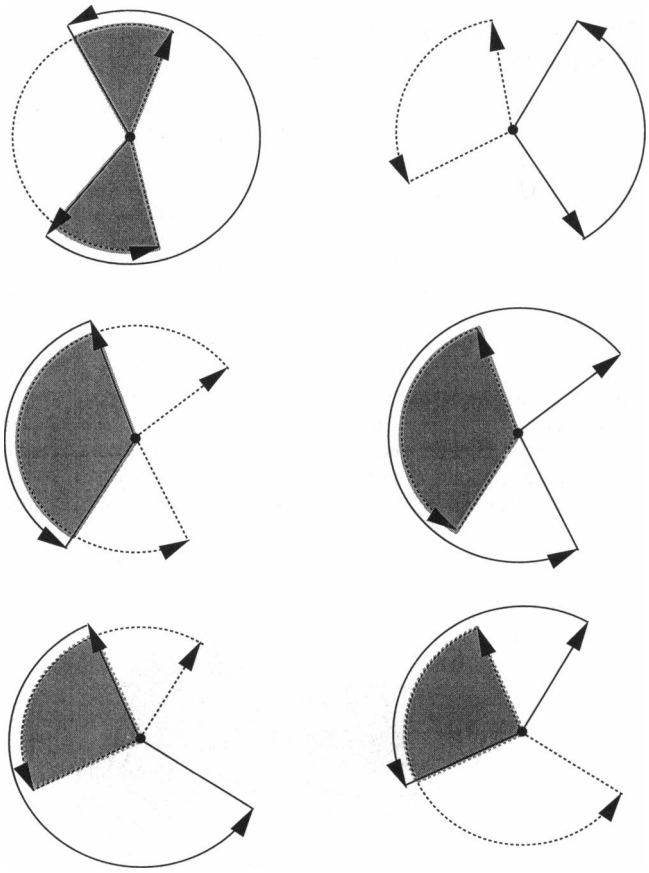

FIGURE 3 The six possible relative locations of two exterior arcs on an intersection circle. The jth arc is drawn as a solid line and the j'th arc is drawn as a dashed line. For clarity, the radius of the j'th arc is slightly reduced. The starting and ending points of each exterior arc are marked by lines starting from the center of the intersection circle (*black dot*) with and without an arrow, respectively. The common parts of the two arcs are not buried in either sphere l' or sphere l and are marked by shades.

Generation of exposed spherical polygons

The exposed arcs make up the boundaries of the exposed patches (spherical polygons) of individual spheres. As illustrated in Fig. 4, two exposed arcs (e.g., the jth and j'th) of sphere n are adjacent to each other on the boundary of an exposed spherical polygon if $a_0(n, j) = a_1(n, j')$ and $a_2(n, j) = a_0(n, j')$. In this way, all the exposed arcs are sorted into disconnected boundaries. If the jth exposed arc of sphere n is used in starting a boundary, then this boundary is closed by an exposed arc (say, the j''th) that has $a_0(n, j'') = a_1(n, j)$ and $a_2(n, j'') = a_0(n, j)$. A completely exposed intersection circle is a boundary by itself. Each boundary on sphere n cuts the whole surface of the sphere into two complementary parts; the part that is exposed is in the positive direction when the boundary is traced from the starting point of one arc to the starting point of the adjacent arc, and the right-hand rule is used (see Fig. 4).

There is the possibility that two or more disconnected boundaries actually form the boundary of a single exposed spherical polygon, as illustrated in Fig. 5. A characteristic of this situation is that each constituent boundary is inside the spherical polygons defined by the other constituent boundaries. One can test whether a point P is inside a spherical polygon by starting a curve on the spherical surface from this point. Let $\mathbf{n}_c$ be the tangential vector of the curve at the point where the boundary of the spherical polygon is first crossed (directed away from P) and $\mathbf{n}_a$ be the tangential vector of the crossed arc at the crossing point (directed away from the starting point of the arc). If $\mathbf{n}_c \times \mathbf{n}_a$ is directed away from the center of the sphere, then P is inside the spherical polygon; otherwise it is outside. In this way all the boundaries on sphere n are tested to see if they are inside each other's spherical polygons. For each group of such boundaries, the arcs of the individual boundaries are collected together. This collection of arcs makes up the boundary of a single exposed spherical polygon.

Sorting of exposed polygons into disconnected surfaces

If two exposed spherical polygons share an arc, then they are adjacent to each other on a closed surface. Consider two arcs. The first is on the intersection circle of sphere n with sphere a_0 and its starting and ending points are further in contact with spheres a_1 and a_2, respectively. The

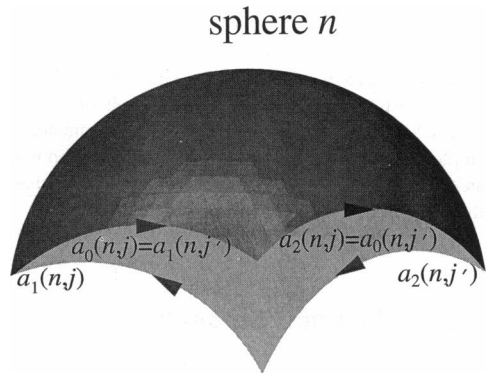

FIGURE 4 The exposed arcs that make up the boundary of an exposed spherical polygon. The jth and j'th exposed arcs of sphere n are in the front, and two unnamed exposed arcs are in the back. When the boundary is traced from the starting point of the jth arc to the starting point of the j'th arc and finally back to the starting point of the jth arc (as shown by the arrows) and the right-hand rule is used, the exposed spherical polygon is in the positive direction.

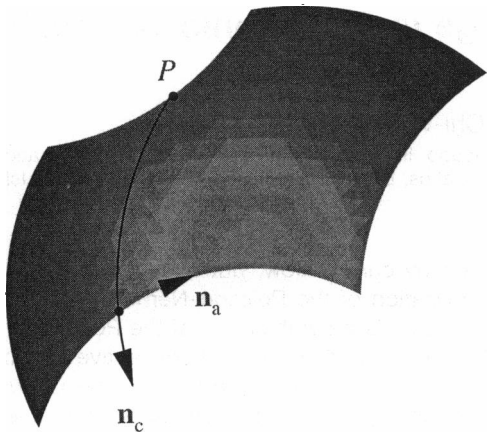

FIGURE 5 An exposed spherical polygon formed by two disconnected boundaries. Each constituent boundary is inside the spherical polygon defined by the other constituent boundary. When a curve started from point P on one boundary is continued until it crosses the other boundary, the cross-product $\mathbf{n}_c \times \mathbf{n}_a$ is directed away from the center of the sphere.

second is on the intersection circle of sphere n' with sphere a_0' and its starting and ending points are in further contact with spheres a_1' and a_2', respectively. If $n = a_0'$, $a_0 = n'$, $a_1 = a_2'$, and $a_2 = a_1'$, then the two arcs are the same arc shared by the spherical polygons whose boundaries contain the two arcs. By testing the arcs making up the boundaries in the above manner, the exposed spherical polygons can be sorted into disconnected sets. Each set constitutes a closed surface.

Selection of the outer surface

Finally, the outer surface is selected by the fact that it consists of the largest number of exposed spherical polygons.

Note added in proof: While this paper was in the review process, N. Tjandra, S. E. Feller, R. W. Pastor, and A. Bax submitted a paper to *J. Am. Chem. Soc.*, in which the authors compared the experimentally determined rotational diffusion tensor of human ubiquitin with that calculated by including explicit water molecules and treating heavy atoms as small beads. Agreement was found when 202 water molecules were included. Using the molecular weight of human ubiquitin (~8560), we can estimate the hydration level to be 0.42. This again confirms the unified picture of protein hydration.

REFERENCES

Alard, P., and S. J. Wodak. 1991. Detection of cavities in a set of interpenetrating spheres. *J. Comp. Chem.* 12:918–922.

Allison, S. A., and V. T. Tran. 1995. Modeling the electrophoresis of rigid polyions: application to lysozyme. *Biophys. J.* 68:2261–2270.

Bull, H. B., and K. Breese. 1968. Protein hydration. II. Specific heat of egg albumin. *Arch. Biochem. Biophys.* 128:497–502.

Buzzell, J. G., and C. Tanford. 1956. The effect of charge and ionic strength on the viscosity of ribonuclease. *J. Phys. Chem.* 60:1204–1207.

Creeth, J. M. 1958. Studies of free diffusion in liquids with the Rayleigh method. III. The analysis of known mixtures and some preliminary investigations with proteins. *J. Phys. Chem.* 62:66–74.

Diamond, R. 1974. Real-space refinement of the structure of hen egg-white lysozyme. *J. Mol. Biol.* 82:371–391.

Ehrenberg, A. 1957. Determination of molecular weights and diffusion coefficients in the ultracentrifuge. *Acta Chem. Scand.* 11:1257–1270.

Kuntz, I. D., Jr. 1971. Hydration of macromolecules. III. Hydration of polypeptides. *J. Am. Chem. Soc.* 93:514–516.

Kuntz, I. D., Jr., and W. Kauzmann. 1974. Hydration of proteins and polypeptides. *Adv. Protein Chem.* 28:239–345.

Luzzati, V., J. Witz, and A. Nicolaieff. 1961. Determination de la masse et des dimensions des proteines en solution par la diffusion centrale des rayons X mesurée à l'échelle absolue: exemple du lysozyme. *J. Mol. Biol.* 3:367–378.

Partington, J. R. 1951. An Advanced Treatise on Physical Chemistry, Vol. 2. Longmans, London. 108–109.

Philips, S. E. V. 1986. Structure and refinement of oxymyoglobin at 1.6 Å resolution. *J. Mol. Biol.* 142:531–554.

Richards, F. M., and H. W. Wyckoff. 1971. Bovine pancreatic ribonuclease. *In* The Enzymes, Vol. 4. P. D. Boyer, editor. Academic Press, New York. 647–806.

Rupley, J. A., and G. Careri. 1991. Protein hydration and function. *Adv. Protein Chem.* 41:37–172.

Rupley, J. A., E. Gratton, and G. Careri. 1983. Water and globular proteins. *Trends Biochem. Sci.* 8:18–22.

Scheraga, H. A. 1961. Protein Structure. Academic Press, New York. 18–19.

Schwert, G. W. 1951. The molecular size and shape of the pancreatic proteases. II. Chymotrypsinogen. *J. Biol. Chem.* 190:799–806.

Sophianopoulos, A. J., C. K. Rhodes, D. N. Holcomb, and K. E. van Holde. 1962. Physical studies of lysozyme. I. Characterization. *J. Biol. Chem.* 237:1107–1112.

Squire, P. G., and M. E. Himmel. 1979. Hydrodynamics and protein hydration. *Arch. Biochem. Biophys.* 196:165–177.

Steinbach, P. J., and B. R. Brooks. 1993. Protein hydration elucidated by molecular dynamics simulation. *Proc. Natl. Acad. Sci. USA.* 90: 9135–9139.

Tanford, C. 1968. Protein denaturation. *Adv. Protein Chem.* 23:121–282.

Venable, R., and R. W. Pastor. 1988. Frictional models for stochastic simulations of proteins. *Biopolymers.* 27:1001–1014.

Wang, D., W. Bode, and R. Huber. 1985. Bovine chymotrypsinogen A. X-ray crystal structure analysis and refinement of a new crystal form at 1.8 Å resolution. *J. Mol. Biol.* 185:595–624.

Wilcox, P. E., J. Kraut, R. D. Wade, and H. Neurath. 1957. The molecular weight of α-chymotrypsinogen. *Biochim. Biophys. Acta.* 24:72–78.

Wlodawer, A., L. A. Svensson, L. Sjolin, and G. L. Gilliland. 1988. Structure of phosphate-free ribonuclease A at 1.26 Å. *Biochemistry.* 27:2705–2717.

Wyman, J., Jr., and E. N. Ingalls. 1943. A nomographic representation of certain properties of the proteins. *J. Biol. Chem.* 147:297–318.

Zhou, H.-X. 1993. Boundary element solution of macromolecular electrostatics: interaction energy between two proteins. *Biophys. J.* 65: 955–963.

Zhou, H.-X. 1994. Macromolecular electrostatic energy within the nonlinear Poisson-Boltzmann equation. *J. Chem. Phys.* 100:3152–3162.

Zhou, H.-X. 1995. Calculation of translational friction and intrinsic viscosity. I. General formulation for arbitrarily shaped particles. *Biophys. J.* 69:2277–2288.